Current Research in Green and Sustainable Chemistry 5 (2022) 100245

Contents lists available at ScienceDirect

Current Research in Green and Sustainable Chemistry

journal homepage: www.elsevier.com/journals/current-research-in-green-and-sustainable-chemistry/2666-0865

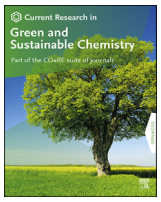

Ligand exchange reactions and PEG stabilization of gold nanoparticles

Charitha Thambiliyagodage

Faculty of Humanities and Sciences, Sri Lanka Institute of Information Technology, Malabe, Sri Lanka

ARTICLE INFO

Keywords:
Ligands
Replacement
Citrate
mPEGSH
SERS

ABSTRACT

Gold nanoparticles (Au NPs) were synthesized by the citrate reduction method. Au NPs were aggregated when mixed with mercaptoethanol (ME), dopamine (DAH) and adenine (AD) as the surface passivating citrate molecules were incompletely but heavily replaced by them as supported by the occurrence of a new peak at a longer wavelength and eventual disappearance of the peak/s in the UV–Visible spectra due to the settlement of the aggregated NPs. Transmission electronic microscopic (TEM) images showed aggregated NPs. AD was increasingly replaced by an increasing concentration of dithiothreitol (DTT) in the range of 20 μM–10 mM, but an incomplete replacement was resulted even after using highly concentrated DTT (10 mM). mPEGSH passivates the gold surface where they bind to the gold surface via a mushroom-like configuration. mPEGSH stabilizes the Au NPs preventing aggregation upon mixing with ME, DAH and AD, as revealed by no change in the position and the absorbance of the localized resonance surface plasmon peak in the UV–Visible spectra and well-dispersed Au NPs in the TEM images. Mushroom-like arrangement of mPEGSH on the Au NPs allow adsorption of ME, DAH and AD as revealed by the surface enhanced Raman spectroscopic data.

1. Introduction

Metal nanoparticles exhibit advantageous properties compared to their bulk counterpart due to their high surface area to volume ratio [1,2] including but not limited to optical properties [1,3], electronic properties [4,5] and magnetic properties [6,7]. Metal nanoparticles such as gold, silver and copper exhibit surface plasmon resonance (SPR) where the electrons in the metal surface layer are excited by photons of incident light with a certain angle of incidence, and then propagate parallel to the metal surface [8]. Metal nanoparticles tend to aggregate and lose their properties. Hence, nanoparticles should be kept in dispersed solutions. Noble metal nanoparticles especially Au NPs are kept in citrate solution [9] or react with thiolated molecules [10].

Stabilization of Au NPs by mixing with PEG called PEGylation is quite known in the world [11–13]. PEG is a water-soluble polymer and it binds with water via hydrogen bonds [14]. PEG is a biocompatible polymer that readily interacts with Au NPs stabilizing them in vivo and in vitro, triggering its applicability especially for in vivo applications such as drug delivery [15,16]. Au NPs tend to aggregate upon exposure to different factors such as the solvent [17], ionic strength [17], foreign molecules [18], temperature [19] etc. Causing them incompatible to be used for different applications. PEG stabilizes Au NPs preventing them from aggregation.

In this study, we report the effect of Mercaptoethanol, Dopamine and Adenine on the aggregation of Au NPs which are biologically important molecules. Mercaptoethanol is widely used in molecular biological applications, dopamine as a neurotransmitter, and adenine as a nitrogenous base. They were selected as they are soluble in water, UV–Visible active due to their structural properties, and represent biologically active molecules with thiol and amine functional groups which have different affinities to the gold surface. However, as Au NPs tend to aggregate upon mixing with these ligands the purpose of using Au NPs is narrowed or even diminished. Therefore, to improve the usability and the applicability of the Au NPs, they were stabilized by mPEGSH where no aggregation was resulted even after mixing with the above ligands. These ligands are adsorbed to the gold surface even in the presence of mPEGSH as it has a mushroom-like configuration where the gold surface is vacant below the cap of the mushroom and between the stems.

2. Materials and methods

2.1. Materials

$HAuCl_4 \cdot 3H_2O$, Trisodium citrate, Mercaptoethanol, Dopamine hydrochloride, Adenine and Methoxy Polyethylene glycol thiol (mPEGSH) (MW = 5000) were purchased from Sigma Aldrich, UK. Nanopure (18 MΩ-cm) water was used for all the experiments.

E-mail address: charitha.t@sliit.lk.

https://doi.org/10.1016/j.crgsc.2021.100245
Received 5 November 2021; Received in revised form 19 December 2021; Accepted 19 December 2021
Available online 22 December 2021

2.2. Synthesis of Au nanoparticles

$HAuCl_4$ (0.0415g) was dissolved in 100 ml of nanopure water and was brought to a boil. Trisodium citrate (0.1141 g) dissolved in 10 ml of nanopure water was added to the above solution. Then the mixture was boiled for another 20 min and was allowed to cool to room temperature.

2.3. ME, DAH and AD adsorption onto Au NPs

Colloidal Au NPs (1 ml) was mixed with 2 ml of ME (28.74 μM), dopamine (50 μM) and adenine (18.16 μM) separately in a cuvette and the time-resolved UV–Visible spectra were collected.

2.4. Stabilization of Au NPs with mPEGSH

Au NPs were mixed with mPEGSH (MW- 5000) for 6 h. Then 1 ml of Au-mPEGSH was mixed with 2 ml of ME, DAH and AD as shown in the previous section separately in a cuvette and the time-resolved UV–Visible spectra were collected.

3. Characterization methods

The morphology of the synthesized nanocomposites was characterized by transmission electron microscopy (TEM). The microscope was operated at 200 kV (JEOL - JEM – 2100). The sample (1 μl) was mounted on a holey carbon copper grid and allowed to dry at room temperature before TEM analysis. Raman analysis was performed by a Bruker Senterra Raman microscope spectrophotometer using 633 nm laser excitation. Surface enhanced Raman spectra were acquired using aggregated Au NPs. The UV–Visible spectroscopic analysis was performed by a Shimadzu UV-1990 double beam UV–Visible spectrophotometer. Nanopure water (18 MΩ-cm) was prepared by a Thermo Scientific nanopure water purification system.

4. Results and discussion

4.1. Ligand exchange reactions

Au NPs synthesized by citrate reduction methods where citrate ions act as the reducing agent and a surface passivating agent. Synthesized spherical NPs were about 12 nm on average and were monodispersed as shown in the TEM image (Fig. 1 (a)) and the histogram (Fig. 1 (b)). The UV–visible spectrum of the synthesized NPs (Fig. 1 (c)) shows a peak at 520 nm indicating the localized surface plasmonic resonance absorption.

This study demonstrates the effect of different ligands on the stability of the Au NPs. ME, DAH, AD, DTT and mPEGSH were selected as the model ligands and their chemical structures are shown in Table 1. Upon addition of ME, a new peak at 720 nm was seen in the UV–Visible spectrum in addition to the peak initially observed at 520 nm (Fig. 2 (a)). The peak at 720 nm indicates the formation of larger nanoparticles. Upon addition of ME, in 2 s absorbance at 520 nm dropped from 2.27 to 2.02 and the absorbance of 720 nm increased to 0.17. After the next 2 s, respective absorbance values are 1.81 and 1.54, while those at 6 s are, 1.53 and 2.15. However, absorbance at 720 nm started to decrease after 6 s (2.01 at 8 s) (Fig. 2 (b)). This indicates that the rate of aggregation of AuNPs is very high in the first 4 s which gets slower in the next 4 s. The reduction of the absorbance at 720 nm after 8 s indicates that the rate of settlement of the nanoparticles is higher than the rate of aggregation. However, the rate of reduction of absorbance at 520 nm (0.06 s^{-1}) is lower than the rate of increase in the absorbance at 720 nm (0.42 s^{-1}). After 360 s which is half of the total experimental time absorbance at 520 nm (0.094) is greater than the absorbance at 720 nm (0.087). After 720 s absorbance at 520 nm (0.026) is greater than the absorbance at 720 nm (0.017). The ratio of absorbance at 520 nm/Absorbance at 720 nm (A_{520}/A_{720}) at 2 s, 4s, 10 s, 360 s and 720 s are, 36.10, 11.37, 0.65, 1.08 and 1.52, respectively, where the absorbances at both wavelengths were equal (ratio = 1) after 612 s. This observation suggests that the citrate replacement by ME does not prominently occur in the first 2 s and become more significant after 2 s of mixing. The ratio decreased till 612 s and started to increase at 614 s which continued until 720 s. This indicates that even after 720s dispersed AuNPs are present in the medium. This observation suggests that all citrate molecules on AuNPs have not been replaced by ME being consistent with the reported data [20,21]. ME has replaced 98.2% of citrate molecules by the formation of the self-assemble monolayers (SAM) where about 1.2% of citrate molecules

Table 1
Chemical structures of the ligands.

Ligand	Structure
Mercaptoethanol	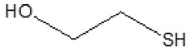
Adenine	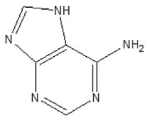
Dopamine	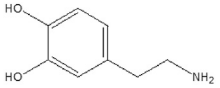
Dithiothreitol	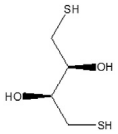
Methoxy Polyethylene Glycol Thiol	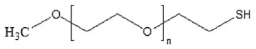

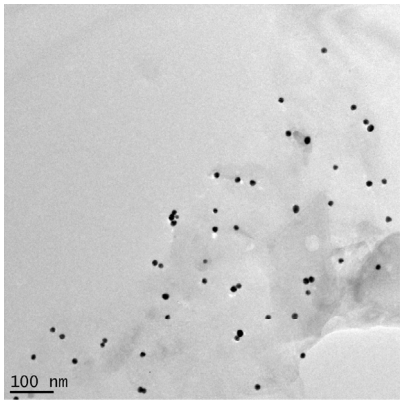

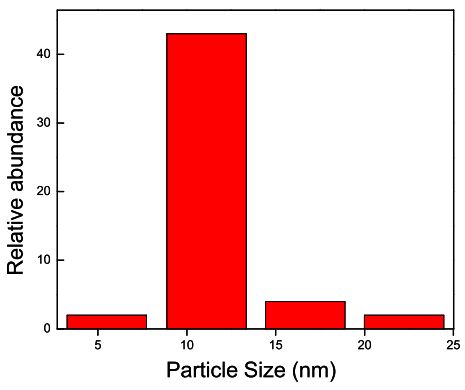

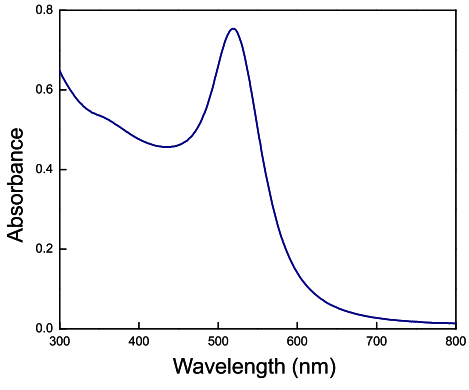

Fig. 1. (a) TEM image (b) Particle size distribution (c) UV–Visible spectrum of Au NPs.

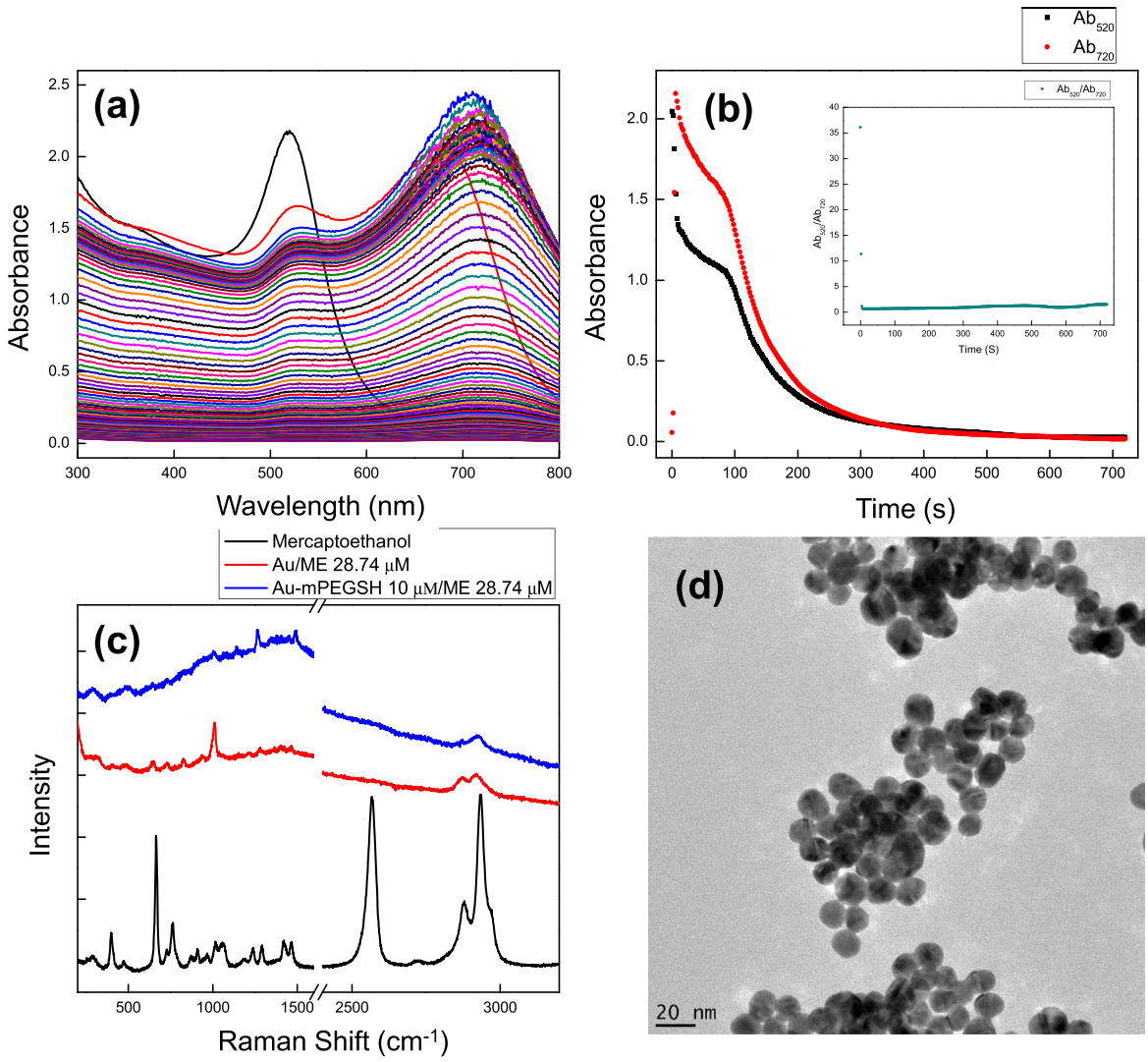

Fig. 2. (a) Time-resolved UV–Visible spectra of Au-ME system (b)Variation of absorbance with time (insert-the variation of A_{520}/A_{720} with time) (c) Raman spectra of ME, Au-ME and Au-mPEGSH (d) TEM images of Au-ME.

are remaining on the gold surface. The bond energy of Au–S (31 kcal/-mol) is much higher than that of Au–COO^- (2 kcal/mol) [22–24]. The binding energy of citrate on the AuNPs depends on the surface coverage [21]. At higher coverages citrate binds to the gold surface through a monocarboxylic monodentate linkage and the displacement of citrate is easier. But at lower coverages, the binding mode of citrate changed to dicarboxylate bridging which exhibited binding energy of 55 kcal/mol and the displacement even by thiols are harder [25]. Therefore, as most of the citrate molecules were replaced by ME it could be assumed that in the synthesis of AuNPs citrate molecules cover more of the gold surfaces. The citrate band (symmetric COO^- stretch) which is supposed to be at 1376 cm^{-1} is not visible in the SERS spectrum of Au- ME due to the insufficiency of citrate present to generate a peak (Fig. 2 (c)). SERS of ME adsorbed to AuNPs compared to the Raman spectrum of pure ME clearly shows the absence of the S–H stretching mode at 2570 cm^{-1} confirming the binding of ME to the gold surface via S–H bond. The Raman shifts of C–S trans and gauche rotational isomers observed in the ME Raman spectrum at 766 and 662 cm^{-1}, respectively, and have shifted to lower Raman shifts as 728 and 647 cm^{-1}, respectively. These shifts imply the withdrawal of electrons from the C–S bond and a concomitant increase in the effective mass in the sulfur atom due to the interactions with the gold surface [26]. TEM image of the settled nanoparticles after mixing with ME (Fig. 2 (d)), was collected to study any change in the morphology of the nanoparticles after the addition of the ligands. TEM image shows aggregated Au NPs and the remaining low amount of dispersed citrate stabilized AuNPs are not present. As they are present in a lower quantity and as TEM is a localized effect such dispersed nanoparticles could not be seen.

The behaviour of the UV–Visible spectra upon addition of Dopamine is shown in Fig. 3 (a). Upon addition of DAH, a new peak at 690 nm appeared with high intensity. However, being different to the behaviour of the UV–Visible spectrum of the Au-ME system, the appearance of the peak at a longer wavelength (690 nm) was comparatively slower. Absorbance at 690 nm in the first 2 s was 0.14 which gradually increased to a maximum of 1.67 in 16 s due to the aggregation of nanoparticles. However, after 16 s absorbance at 690 nm decreased as the rate of settlement of nanoparticles is lower than the rate of aggregation. The rate constant of increase in absorbance at 690 nm is 0.35 s^{-1} which is lesser than with ME (0.42 s^{-1}). The rate of reduction of the absorbance at 520 nm (0.05 s^{-1}) is lower than that with ME (0.06 s^{-1}). Absorbance at 520 nm decreased to 1.53 in 6 s with ME, however, to reach the same absorbance 14 s was consumed with DAH. This indicates that the aggregation of AuNPs upon addition of DAH is slower than with ME and hence the rate of citrate replacement is also lower than that with ME. The ratio of absorbance at 520 nm to the absorbance at 690 nm (A_{520}/A_{690}) right after 2, 4, 10, 360 and 720 s are 14.62, 2.41, 1.01, 0.91 and 1.10, respectively (Fig. 3(b)). A_{520}/A_{690} after 2, 4 s are

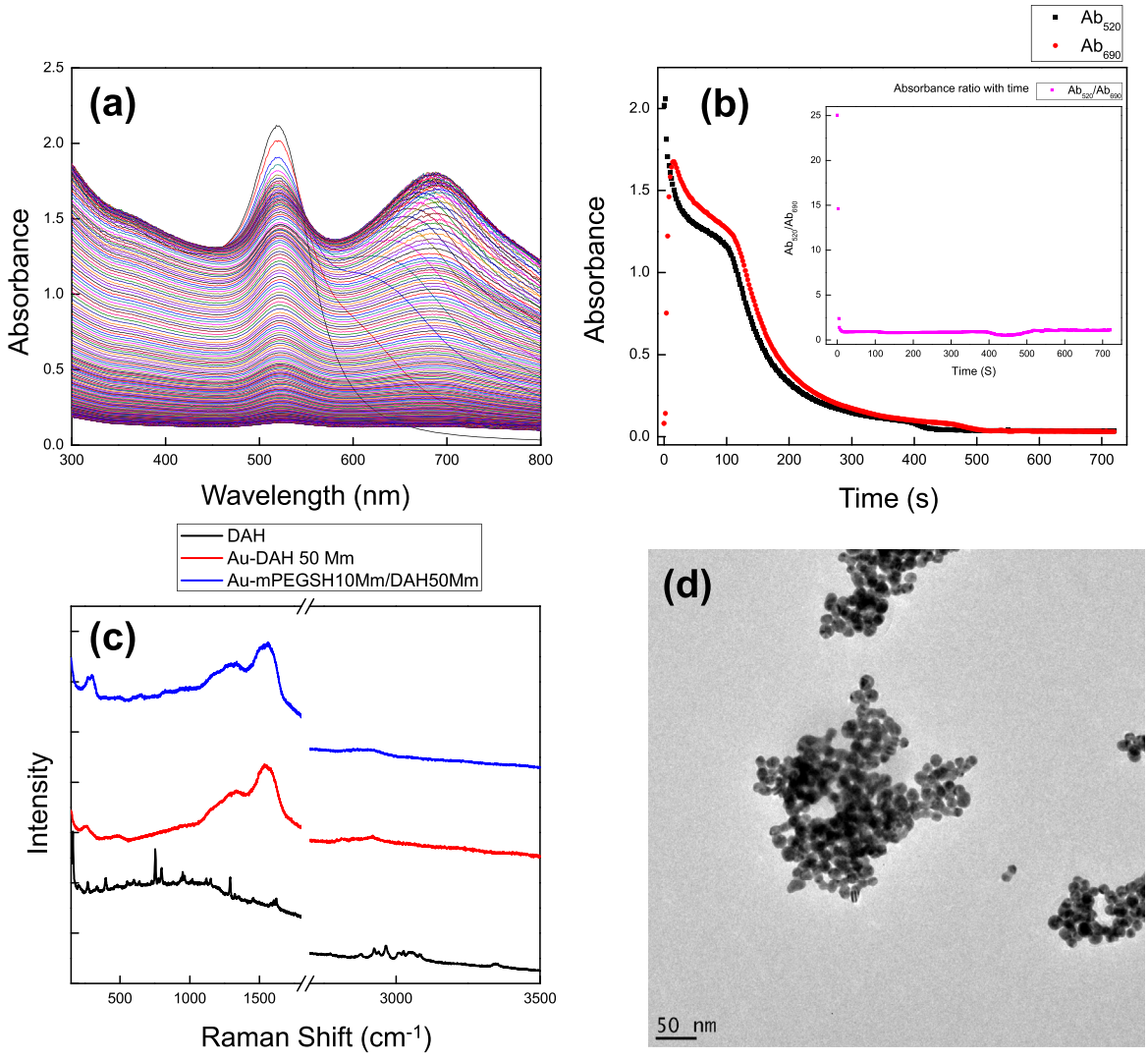

Fig. 3. (a) Time-resolved UV–Visible spectra of Au-DAH system (b)Variation of absorbance with time (insert-the variation of A_{520}/A_{690} with time) (c) Raman spectra of DAH, Au- DAH and Au-mPEGSH (d) TEM images of Au- DAH.

lesser than that resulted with ME. The ratio reached 1.00 in 10 s which is a lot lesser than that with ME (612 s). These results suggest that the rate of aggregation of AuNPs in the presence of DAH is much lower than with ME. Further, the ratio increased to a maximum of 1.10 after 720 s being different to the behaviour in the presence of ME where the ratio increased a maximum of 1.52 at the same time. This indicates that the concentration of the dispersed nanoparticles is 1.01 times higher than the concentration of the aggregated nanoparticles after 720 s which is lesser than that with ME. This suggests that though the rate of aggregation of AuNPs in the presence of DAH is lesser than in the presence of ME, the amount of AuNPs aggregated with DAH is higher than that with ME. TEM image (Fig. 3(c)) also show aggregated nanoparticles. SERS spectrum (Fig. 3(d)) shows the prominent broad bands at 1345 cm^{-1} and 1552 cm^{-1} caused by the deformations of the catechol ring [27]. This indicates that DAH doesn't form interactions with the gold surface via OH significantly. However, Raman bands appeared in the region of 2864–3092 cm^{-1} which correspond to CH_3 symmetric and antisymmetric stretching frequencies, and the broadband in the region of 3324–3364 cm^{-1} attributed to NH_2 symmetric and antisymmetric frequencies are not present in the SERS of Au-DAH [28]. This suggests that DAH interacts with the gold surface via the NH_2 group.

To further study the effect of amine-containing ligands AuNPs were mixed with Adenine. It was observed that upon addition of Adenine a new peak at a longer wavelength (680 nm) appeared in addition to the peak at 520 nm indicating the formation of larger nanoparticles (Fig. 4(a)). Absorbance at 680 nm in the first 2 s increased to 1.82 which increased to 2.51 in 8 s due to the aggregation of nanoparticles being consistent with ME and DAH and the absorbance started to decrease after that as the nanoparticles started to settle in the cuvette. The rate of increase of the absorbance at 680 nm is 0.05 s^{-1} which is lower than that with both ME and DAH. The rate of reduction of the absorbance at 520 nm (0.04 s^{-1}) is lower than that with ME and DAH. Absorbance at 520 nm decreased to 1.53 in 6 s and 14 s, with ME and DAH, respectively, and to reach the same absorbance with AD, 46 s was spent. This observation suggests that the rate of aggregation of AuNPs upon addition of adenine is lower than that with ME and DAH. As the absorbance at 680 nm reached 0.01 in 472 s the whole experiment was conducted for 496 s only. The ratio of absorbance at 520 nm to the absorbance at 680 nm (A_{520}/A_{680}) right after 2, 4, 10, 360 and 496 s are 1.12, 0.81, 0.73, 2.53 and 148.43, respectively (Fig. 4 (b)). A_{520}/A_{680} ratio after 2 and 4 s are lower than those with ME and DAH. Equal concentrations of both dispersed and aggregated nanoparticles ($A_{520} = A_{680}$) were observed at 180 s which is a lot before with ME (612 s) and after with DAH (10 s). Moreover, the ratio increased to 10 after 462 s and reached 148.43 after the completion of the reaction (496 s). As stated above the absorbance at 680 nm decreased to 0.01 in 472 s, and absorbance values resulting after

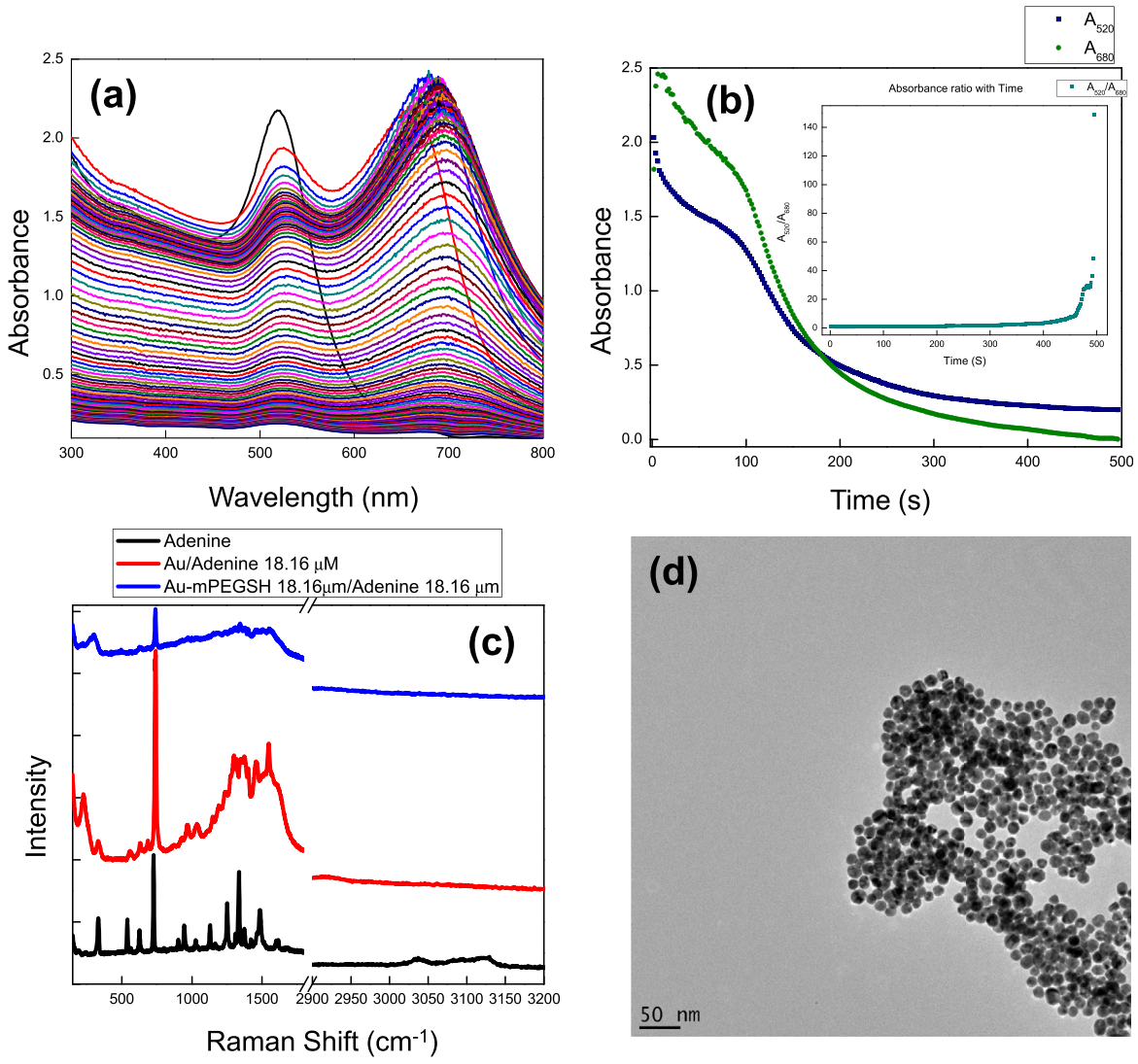

Fig. 4. (a) Time-resolved UV–Visible spectra of Au-AD system (b)Variation of absorbance with time (insert-the variation of A_{520}/A_{690} with time) (c) Raman spectra of AD, Au - AD and Au-mPEGSH (d) TEM images of Au- AD.

that are very low indicating the absence of aggregated larger nanoparticles in the solution and the presence of dispersed AuNPs stabilized by citrate in the solution. Further, this observation also supports the fact that citrate molecules cannot be replaced totally. TEM image (Fig. 4 (c)) further shows aggregated AuNPs. SERS of Au-AD is shown in Fig. 4 (d). The peak with the highest intensity at 720 cm^{-1} of the Raman spectrum of AD corresponds to the breathing mode of Adenine shifts to 742 cm^{-1} in SERS of Au-AD [29]. Symmetric and antisymmetric frequencies of NH_2 of the Raman spectrum of AD are absent in SERS of Au-AD indicating that AD interacts with the gold surface via the NH_2 group. Moreover, among the nitrogen-containing ligands dopamine is more effective in replacing citrate than adenine. This could be described by the structural differences of DAH and AD. NH_2 group of DAH is present at the end of the substituent and easily they can form SAM and occupy the surface of the AuNPs. However, AD is a heterocyclic compound where four nitrogens are present in the two rings, and the NH_2 is attached as a substituent. Therefore, there are multiple binding sites in AD and hence though they interact with Au NP surface nanoparticle surface cannot be covered with AD. Hence, more citrate molecules can remain on the nanoparticle surface as shown above. Interestingly, both ME and DAH have hydroxyl groups as well which may be for weaker interactions with the Au surface. The binding energy of Au–NH_2 (8 kcal/mol) is greater than that of Au-citrate (2 kcal/mol) [21,22]. Therefore, the replacement of citrate molecules with N containing ligands is feasible.

Ligand replacement on Au NPs was further studied. AD replacement by Dithiothreitol (DTT) was used as an example. DTT was selected as it bears two thiol groups. The binding affinity of thiol to Au NP surface is higher than other functional groups. Therefore, it is hypothesized that DTT would efficiently remove amine functionalized AD. Au NPs when mixed with AD aggregated and settled in the cuvette as explained above. Those aggregated NPs were isolated and DTT in varying concentrations (20 μM, 100 μM, 500 μM, 1 mM and 10 mM) were added to such aggregated NPs separately. As exhibited in the UV–Visible spectra (Fig. 5 (a)) it could be seen that the absorbance of the characteristic peak of AD at 260 nm increased with increasing concentration of DTT where with 20 μM insignificant AD desorption ($A_{260} = 0.005$) was observed while with 10 mM ($A_{281} = 0.16$) significant AD desorption was obtained, which is 32 times of the desorption resulted with 20 μM DTT. The wavelength at maximum absorbance (λ_{max}) shifted to higher wavelengths where it was 260 nm with 20 μM DTT and 281 nm with 10 mM DTT. This could be due to the interactions of the free DTT in the solution and the desorbed AD. It is quite interesting that when an equal concentration of DTT is added to the aggregated AuNPs negligible amount of AD was desorbed and significant AD desorption was obtained only when a very high

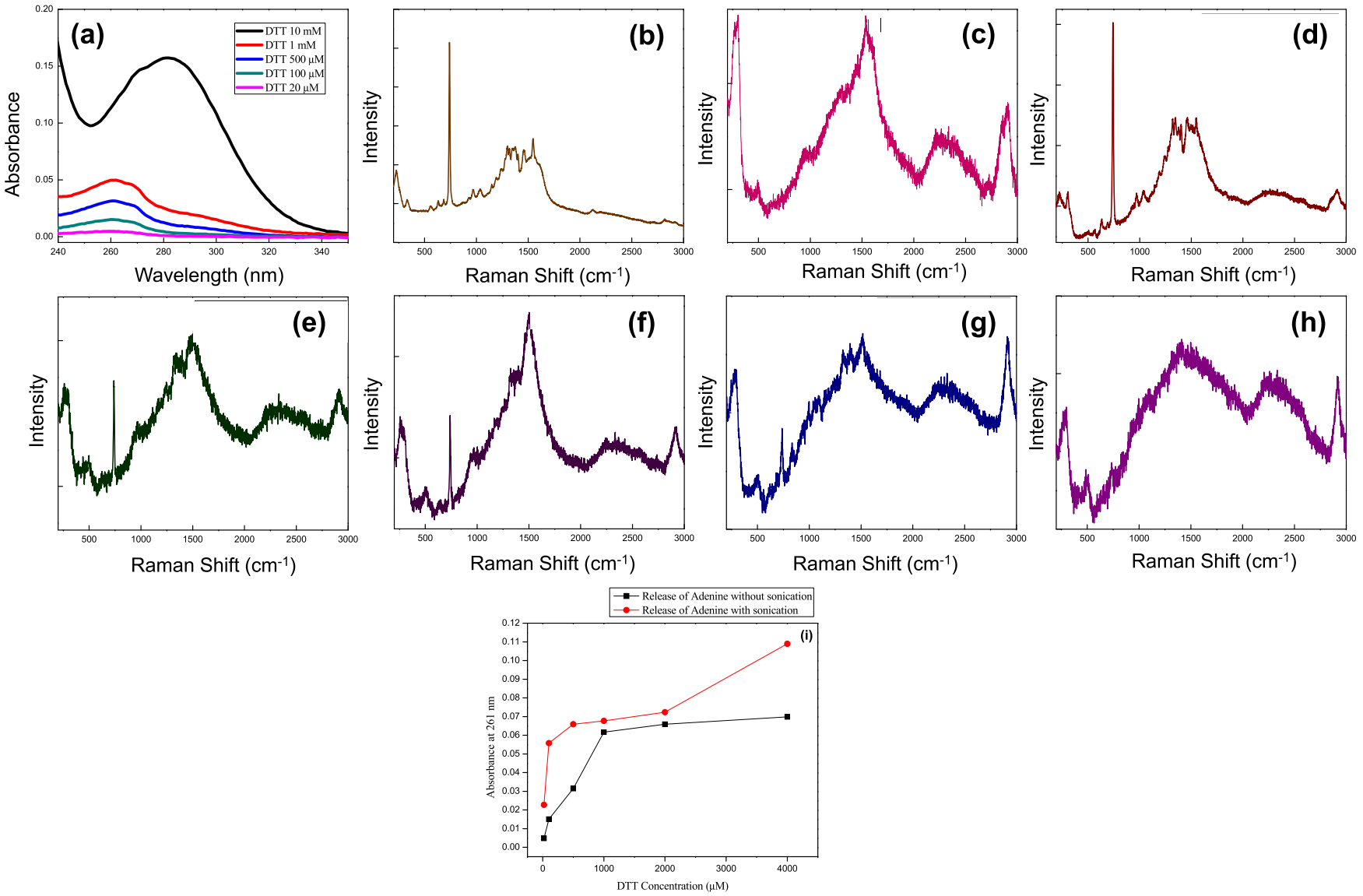

Fig. 5. (a) Replace of AD with increasing concentration of DTT, SERS spectra of (b) Au-AD (c) Au-DTT, SERS spectra showing the AD replace by different concentrations of DTT (d) 20 µM (e)100 µM (f) 500 µM (g) 1 mM (h) 10 mM (i) effect of sonication on desorption of AD.

concentration of DTT (10 mM) which is 500 times higher than the concentration of AD, was used for the experiment. To study the replacement effect further, SERS spectra of aggregated Au NPs after adding DTT were collected (Fig. 5). The characteristic peak of AD (peak with the highest intensity at 742 cm^{-1}) was used to determine the presence of AD on Au NPs (Fig. 5 (b)). It could be seen that the intensity of this peak decreased with increasing concentration of DTT (20 μM, 100 μM, 500 μM, 1 mM and 10 mM, Fig. 5 (d), (e), (f), (g) and (h), respectively). It was clear that though the presence of AD was detected in the UV–Visible spectrum upon addition of increasing concentration of DTT, AD was still present on the gold surface but at lower concentrations, as revealed by the reducing peak intensity at 742 cm^{-1}. Further, though the characteristic features of the SERS of Au-DTT (Fig. 5 (c)) started to be prominent with increasing concentration of DTT, the spectral features of AD especially the peak at 742 cm^{-1} was present but in decreasing amount. Though the SERS spectrum of AD replacement by 10 mM DTT was identical to the spectral features of Au-DTT (Fig. 5 (h)), the peak corresponding to the breathing modes of AD was present in very low intensity, indicating that still there are AD molecules present on the gold surface. Since DTT has two thiol groups and as the binding affinity of SH groups is higher than NH_2, rapid desorption of AD was expected. However, the remaining AD even after adding a very high concentration of DTT suggests that vacant adsorption sites are available on Au NP surface where other ligands could adsorb, and complete ligand desorption is not possible. Further, the effect of sonication on desorption of AD upon addition of DTT was studied (Fig. 5(i)). A negligible amount of AD corresponding to an absorbance of 0.005 was desorbed with 20 μM DTT in the medium and with no sonication. However, in the same medium but in the presence of sonication an amount of AD corresponding to an absorbance of 0.023 was desorbed. Therefore, sonication has facilitated 78.3% desorption of AD. However, though in general the desorption of AD is higher in the presence of sonication, the difference of AD desorption with and without sonication, varied from one DTT concentration to the other. For example, with 100 μM of DTT an amount corresponding to 0.015 of AD was released to the medium without sonication and with sonication an amount of AD corresponding to an absorbance of 0.056 was desorbed in the presence of sonication which is 3.7 times higher than that obtained without sonicating the medium. With 1 mM of DTT, amounts of AD desorbed, with and without sonication are quite similar (amounts corresponding to absorbances of 0.062 and 0.068, respectively). However, with 4 mM of DTT an amount of AD corresponding to an absorbance of 0.07 was released without sonication while, an amount corresponding to an absorbance of 0.109 was released in the presence of sonication which is only a 1.56 times increase compared to the amount desorbed without sonication. Therefore, it could be concluded that the energy provided by sonication facilitates Au-amine bond cleavage.

4.2. mPEGSH stabilization of AuNPs

It could be seen that the intensity of the LSPR peak of the Au NPs mixed with mPEGSH increased from 0.07 (Fig. 6 (a)). Further, the peak position has shifted to the longer wavelength region slightly. This is due to the increase in the dielectric constant of the dielectric shells surrounding the metal surfaces [30,31]. The refractive index of PEGSH (1.46) is higher than that of water (1.33), while the dielectric constant of PEGSH (2.1316) is greater than that of water (1.7689) [32]. Surface modification of Au NPs with mPEGSH was also studied by SERS. The S–H stretching mode at 2580 cm^{-1} present in the Raman spectrum of mPEGSH is absent in the SERS spectrum of Au-mPEGSH indicating the formation of SAM via SH bond. Further, the presence of an Au–S bond at 490 cm^{-1} confirms the formation of SAM of mPEGSH on Au NPs (Fig. 6 (b)). Moreover, the set of peaks present in both spectra in the range of 2890–2950 cm^{-1} correspond to C–H vibration also confirms that mPEGSH has successfully chemically interacted with the gold surface. TEM image (Fig. 6 (c)) shows no considerable nanoparticle aggregation in Au-mPEGSH.

The stability of the Au NPs after the modification with mPEGSH was studied by mixing such modified NPs with ME, DAH and AD, the ligands for which the citrate passivated Au NPs were unstable. Kinetics were studied for the same durations. It was observed that the position of the LSPR peak (520 nm) nor the absorbance was changed for the whole duration tested in ME, DAH and AD (Fig. 7 (a), (b) and (c), respectively). The TEM images collected after completely mixing Au- mPEGSH with the above ligands (Fig. 7 (d), (e), and (f), respectively) show no aggregation of Au NPs further confirming the stabilization of Au NPs by mPEGSH. It was essential to investigate the adsorption of the above three ligands to Au-mPEGSH. Polyethylene glycol is a biocompatible polymer and was selected to stabilize the Au NPs. Meanwhile, the molecules with the desired properties also should bind to the gold surface as it is the main purpose. In this study ligands (ME, DAH and AD) that are biologically important were selected. To study the adsorption of ME, DAH and AD to Au- mPEGSH, SERS spectra were collected (Figure (g), (h) and (i), respectively). All three spectra show the adsorption of the respective ligands identified by the respective characteristic features, in addition to the spectral features of mPEG-SH. However, it was noticed that compared to the respective ligand adsorption to citrate passivated Au NPs, a lesser amount of ligand was adsorbed to Au- mPEGSH. This suggests that adsorption of mPEGSH limits the adsorption of the other ligands studied but does not completely restrict the adsorption as well, being a bulky long-chain molecule. Further, this observation suggests that the total Au NP surface is not covered with mPEGSH because if mPEGSH covers the Au NP surface completely no adsorption of small molecules such as ME, DAH and AD would be observed. Reduced adsorption clearly illustrates that available vacant surface is limited for the adsorption of those

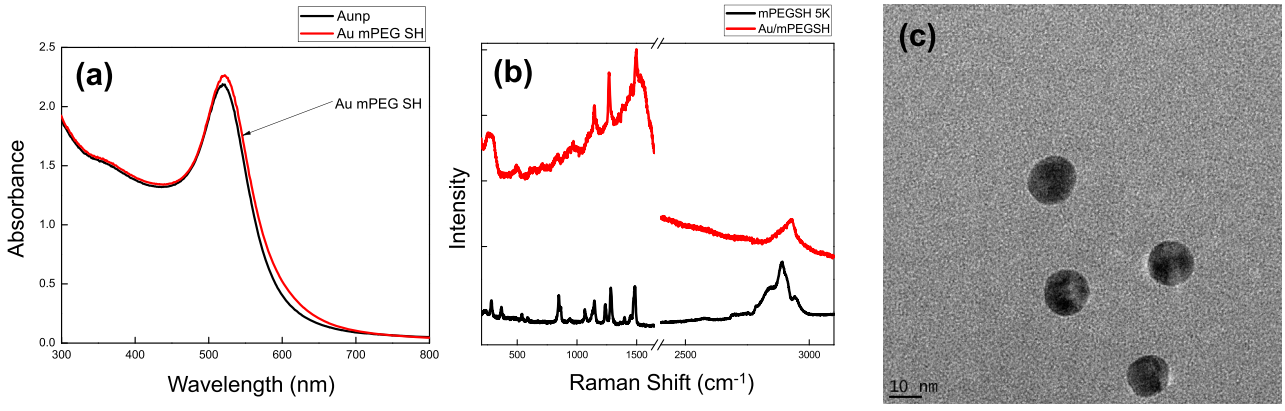

Fig. 6. (a) UV–Visible spectra of Au NPs and Au-mPEGSH (b) SERS spectra of mPEGSH and Au-mPEGSH (c) TEM image of Au-mPEGSH.

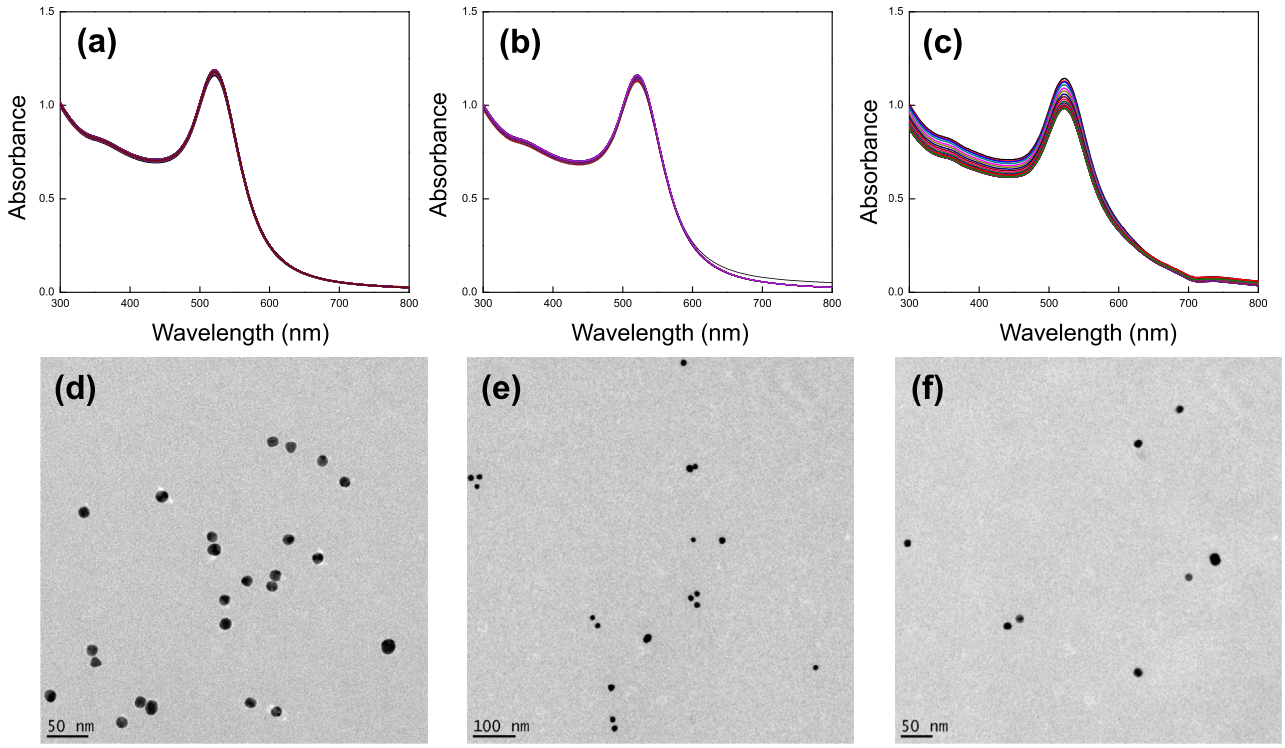

Fig. 7. Time resolve UV–Visible spectra of (a) Au-mPEGSH-ME (b) Au-mPEGSH-DAH (c) Au-mPEGSH-AD, TEM images of (d) Au-mPEGSH-ME (e) Au-mPEGSH-DAH (f) Au-mPEGSH-AD.

molecules. PEG can adsorb to Au NP surface via two conformations: "mushroom" and "brush", depending on the density of PEG. High density PEG favours the brush conformation which is more effective in surface passivation and the low dense PEGylation allows the "mushroom" conformation [33]. Further, the "mushroom" conformation is known establish when the distance between the attachment points of polymer to the surface of the nanoparticle (D) is larger than the Flory radius (F), which depends on the number of monomers per polymer and the length of the monomer. The "brush" like conformation is favoured when such distance is lesser than the Flory radius and when D is approximately similar to F, a transition of mushroom to brush conformation could be resulted [34]. When PEG-SH is adsorbed to the gold surface as a mushroom the space under the cap of the mushroom and in between the stems of the mushrooms are available for the ligands like ME, DAH and AD. It could be argued that the mechanism of the ligand adsorption to AuNP surface could be the replacement of mPEGSH by those ligands. Consequently, then the aggregation of Au NPs should be observed and the spectral features unique to mPEGSH should be absent in the SERS spectrum. However, as both observations were not made mPEGSH replacement mechanism is not applicable. This is due to the low affinity of adenine compared to the thiol functionalized mPEGSH which has a higher binding affinity. Moreover, ME, DAH and AD could be assumed to form interactions with the mPEG-SH molecules bound to the Au NP surface. These interactions could be hydrogen bonds, van Der Waals bonds and electrostatic interactions. However, this mechanism has been ruled out due to the fact that adsorption of adenine decreased and then has reached a plateau with increasing PEG-SH concentration though an increase in adenine adsorption was expected [32]. Therefore, it could be concluded that mPEGSH stabilize the Au NPs and allow adsorption of other ligands as well. Moreover, as ME, DAH and AD adsorbed to the mPEGSH capped Au NPs surface it could be concluded that mPEGSH bound in "mushroom" like conformation because if the mPEGSH bound to the Au NP surface via "brush" like conformation ligands would not be able to bind simultaneously with mPEGSH to the Au NP surface. The mean particle size increases when the Au NPs surface is passivated with PEG. It has been reported that the mean particle size of citrates capped Au NPs increased from 15 nm to 105 nm once passivated with mPEGSH (MW – 48,000 g/mol). The zeta potential was also found to shift from around −35 mV for citrate capped Au NPs to −1 mV for Au-mPEGSH proving that the nanoparticles were successfully capped with a neutral capping agent [34]. A methoxy group is located at the far end of mPEGSH and therefore create repulsion forces between the neutral molecules dispersing the Au NPs preventing the aggregation as resulted with ME, DAH and AD.

5. Conclusions

Au NPs synthesized by citrate reduction method rapidly aggregated upon addition of thiol-containing ligand ME, and amine-containing ligands DAH and AD. However, complete replacement of citrate molecules did not take place. AD was incompletely replaced by DTT as the affinity of thiols is higher than amines. Au NPs were stabilized by mixing with mPEGSH and they were stable against aggregation. mPEGSH modified Au NPs surface by adsorbing via mushroom-like configuration and allowed adsorption of ME, DAH and AD.

Declaration of competing interest

The authors report no conflict of interest.

References

[1] J. Requejo-Isidro, R. del Coso, J. Solis, J. Gonzalo, C.N. Afonso, Role of surface-to-volume ratio of metal nanoparticles in optical properties of Cu:Al_2O_3 nanocomposite films, Appl. Phys. Lett. 86 (19) (May 2005) 193104, https://doi.org/10.1063/1.1923198.

[2] J.N. Sharma, D.K. Pattadar, B.P. Mainali, F.P. Zamborini, Size determination of metal nanoparticles based on electrochemically measured surface-area-to-volume ratios, Anal. Chem. 90 (15) (Aug. 2018) 9308–9314, https://doi.org/10.1021/ACS.ANALCHEM.8B01905.

[3] F. Vallée, Optical properties of metallic nanoparticles, Nanomater. Nanochemistry (2008) 197–227, https://doi.org/10.1007/978-3-540-72993-8_7.

[4] Mathias Brust, Donald Bethell, Christopher J. Kiely, D.J. Schiffrin, Self-assembled gold nanoparticle thin films with nonmetallic optical and electronic properties, Langmuir 14 (19) (Sep. 1998) 5425–5429, https://doi.org/10.1021/LA980557G.

[5] I. Fratoddi, et al., Electronic properties of a functionalized noble metal nanoparticles covalent network, J. Phys. Chem. C 121 (33) (Aug. 2017) 18110–18119, https://doi.org/10.1021/ACS.JPCC.7B07176.
[6] Kyoungja Woo, et al., Easy synthesis and magnetic properties of iron oxide nanoparticles, Chem. Mater. 16 (14) (Jul. 2004) 2814–2818, https://doi.org/10.1021/CM049552X.
[7] Y. Yamamoto, T. Miura, Y. Nakae, T. Teranishi, M. Miyake, H. Hori, Magnetic properties of the noble metal nanoparticles protected by polymer, Phys. B Condens. Matter 329–333 (II) (May 2003) 1183–1184, https://doi.org/10.1016/S0921-4526(02)02102-6.
[8] Y. Zeng, et al., Recent advances in surface plasmon resonance imaging: detection speed, sensitivity, and portability, Nanophotonics 6 (5) (Sep. 2017) 1017–1030, https://doi.org/10.1515/NANOPH-2017-0022.
[9] I. Lázár, H.J. Szabó, Prevention of the aggregation of nanoparticles during the synthesis of nanogold-containing silica aerogels, Vol. 4, Page 55, Gels 2018 4 (2) (Jun. 2018) 55, https://doi.org/10.3390/GELS4020055.
[10] Shishan Zhang, Gyu Leem, La-ongnuan Srisombat, T.R. Lee, Rationally designed ligands that inhibit the aggregation of large gold nanoparticles in solution, J. Am. Chem. Soc. 130 (1) (Jan. 2007) 113–120, https://doi.org/10.1021/JA0724588.
[11] Q.H. Quach, R.L.X. Kong, J.C.Y. Kah, Complement activation by PEGylated gold nanoparticles, Bioconjugate Chem. 29 (4) (Apr. 2018) 976–981, https://doi.org/10.1021/ACS.BIOCONJCHEM.7B00793.
[12] K. Rahme, et al., Highly stable PEGylated gold nanoparticles in water: applications in biology and catalysis, RSC Adv. 3 (43) (Oct. 2013) 21016–21024, https://doi.org/10.1039/C3RA41873A.
[13] R. Stiufiuc, et al., One-step synthesis of PEGylated gold nanoparticles with tunable surface charge, J. Nanomater. 2013 (2013), https://doi.org/10.1155/2013/146031.
[14] K. Li, Y. Qi, Y. Zhou, X. Sun, Z. Zhang, Microstructure and properties of poly(ethylene glycol)-segmented polyurethane antifouling coatings after immersion in seawater, 2021, Vol. 13, Page 573, Polym 13 (4) (Feb. 2021) 573, https://doi.org/10.3390/POLYM13040573.
[15] F. Kawai, Biodegradation of polyethers (Polyethylene glycol, polypropylene glycol, polytetramethylene glycol, and others), Biopolym. Online, Apr. (2001), https://doi.org/10.1002/3527600035.BPOL9012.
[16] K. Knop, R. Hoogenboom, D. Fischer, U.S. Schubert, Poly(ethylene glycol) in drug delivery: pros and cons as well as potential alternatives, Angew. Chem. Int. Ed. 49 (36) (Aug. 2010) 6288–6308, https://doi.org/10.1002/ANIE.200902672.
[17] E. Grueso, P. Perez-Tejeda, R.M. Giráldez-Pérez, R. Prado-Gotor, F. Muriel-Delgado, Ethanol effect on gold nanoparticle aggregation state and its implication in the interaction mechanism with DNA, J. Colloid Interface Sci. 529 (Nov. 2018) 65–76, https://doi.org/10.1016/J.JCIS.2018.05.108.
[18] H.M. Zakaria, A. Shah, M. Konieczny, J.A. Hoffmann, A.J. Nijdam, M.E. Reeves, Small molecule- and amino acid-induced aggregation of gold nanoparticles, Langmuir 29 (25) (Jun. 2013) 7661–7673, https://doi.org/10.1021/LA400582V.
[19] A. Dutta, A. Paul, A. Chattopadhyay, The effect of temperature on the aggregation kinetics of partially bare gold nanoparticles, RSC Adv. 6 (85) (Aug. 2016) 82138–82149, https://doi.org/10.1039/C6RA17561A.
[20] G.S. Perera, S.A. Athukorale, F. Perez, C.U. Pittman, D. Zhang, Facile displacement of citrate residues from gold nanoparticle surfaces, J. Colloid Interface Sci. 511 (Feb. 2018) 335–343, https://doi.org/10.1016/J.JCIS.2017.10.014.
[21] H. Wei, et al., Real-time monitoring of ligand exchange kinetics on gold nanoparticle surfaces enabled by hot spot-normalized surface-enhanced Raman scattering, Environ. Sci. Technol. 53 (2) (Jan. 2018) 575–585, https://doi.org/10.1021/ACS.EST.8B03144.
[22] W. Xi, B.K. Shrestha, A.J. Haes, Promoting intra- and intermolecular interactions in surface-enhanced Raman scattering, Anal. Chem. 90 (1) (Jan. 2017) 128–143, https://doi.org/10.1021/ACS.ANALCHEM.7B04225.
[23] R. Dinkel, B. Braunschweig, W. Peukert, Fast and slow ligand exchange at the surface of colloidal gold nanoparticles, J. Phys. Chem. C 120 (3) (Jan. 2016) 1673–1682, https://doi.org/10.1021/ACS.JPCC.5B11055.
[24] B.M. DeVetter, P. Mukherjee, C.J. Murphy, R. Bhargava, Measuring binding kinetics of aromatic thiolated molecules with nanoparticles via surface-enhanced Raman spectroscopy, Nanoscale 7 (19) (May 2015) 8766–8775, https://doi.org/10.1039/C5NR01006C.
[25] H. Al-Johani, et al., The structure and binding mode of citrate in the stabilization of gold nanoparticles, 2017 99, Nat. Chem. 9 (9) (Mar. 2017) 890–895, https://doi.org/10.1038/nchem.2752.
[26] Vladimir V. Tarabara, Igor R. Nabiev, Alexei V. Feofanov, Surface-enhanced Raman scattering (SERS) study of mercaptoethanol monolayer assemblies on silver citrate hydrosol. Preparation and characterization of modified hydrosol as a SERS-active substrate, Langmuir 14 (5) (Mar. 1998) 1092–1098, https://doi.org/10.1021/LA9709711.
[27] V.K. Thakur, M.-F. Lin, E.J. Tan, P.S. Lee, Green aqueous modification of fluoropolymers for energy storage applications, J. Mater. Chem. 22 (13) (Mar. 2012) 5951–5959, https://doi.org/10.1039/C2JM15665B.
[28] P.K. Kipkemboi, P.C. Kiprono, J.J. Sanga, Vibrational spectra of t-butyl alcohol, t-butylamine and t-butyl alcohol + t-butylamine binary liquid mixtures, Bull. Chem. Soc. Ethiop. 17 (2) (Jan. 2004) 211–218, https://doi.org/10.4314/bcse.v17i2.61689.
[29] M. Pagliai, S. Caporali, M. Muniz-Miranda, G. Pratesi, V. Schettino, SERS, XPS, and DFT study of adenine adsorption on silver and gold surfaces, J. Phys. Chem. Lett. 3 (2) (Jan. 2012) 242–245, https://doi.org/10.1021/JZ201526V.
[30] Linda S. Jung, Charles T. Campbell, Timothy M. Chinowsky, Mimi N. Mar, S.S. Yee, Quantitative interpretation of the response of surface plasmon resonance sensors to adsorbed films, Langmuir 14 (19) (Sep. 1998) 5636–5648, https://doi.org/10.1021/LA971228B.
[31] Michelle Duval Malinsky, K. Lance Kelly, George C. Schatz, Richard P. Van Duyne, Chain length dependence and sensing capabilities of the localized surface plasmon resonance of silver nanoparticles chemically modified with alkanethiol self-assembled monolayers, J. Am. Chem. Soc. 123 (7) (Feb. 2001) 1471–1482, https://doi.org/10.1021/JA003312A.
[32] K. Siriwardana, et al., Ligand adsorption and exchange on pegylated gold nanoparticles, J. Phys. Chem. C 118 (20) (May 2014) 11111–11119, https://doi.org/10.1021/JP501391X.
[33] Y.R. Perera, J.X. Xu, D.L. Amarasekara, A.C. Hughes, I. Abbood, N.C. Fitzkee, Understanding the adsorption of peptides and proteins onto PEGylated gold nanoparticles, 2021, Vol. 26, Page 5788, Mol 26 (19) (Sep. 2021) 5788, https://doi.org/10.3390/MOLECULES26195788.
[34] K. Rahme, L. Chen, R.G. Hobbs, M.A. Morris, C. O'Driscoll, J.D. Holmes, PEGylated gold nanoparticles: polymer quantification as a function of PEG lengths and nanoparticle dimensions, RSC Adv. 3 (17) (Apr. 2013) 6085–6094, https://doi.org/10.1039/C3RA22739A.